Pergamon

Int. J. Solids Structures Vol. 33, No. 27, pp. 3969–3982, 1996

0020-7683/96 $15.00 + .00

0020-7683(95)00220-0

ON THE DIRECT DETERMINATION OF INVARIANT PARAMETERS GOVERNING ANISOTROPIC PLATE BENDING PROBLEMS

M. GRÉDIAC

Ecole Nationale Supérieure des Mines de Saint-Etienne, Sciences des Matériaux et des Structures, Département Mécanique et Matériaux, 158, cours Fauriel, 42023 Saint-Etienne Cedex 2, France

(*Received* 24 *January* 1995; *in revised form* 13 *September* 1995)

Abstract—Many papers deal with the determination of flexural rigidities of anisotropic plates from only one specimen subjected to one or several loading conditions. In such a problem, one of the main questions is the best identification of the unknown parameters according to the type of material, the shape of the specimen and the loading conditions. It seems that no general rule giving the "best" configuration leading to an accurate determination has been established. One of the main reasons is the anisotropic nature of the tested plates, which leads the mechanical configuration to be dependent on the material itself. This problem would be avoided by the direct measurement of invariant parameters from which the rigidities are easily deduced. These invariant parameters reveal the intrinsic elastic behavior of the tested plate, contrary to the rigidities usually considered which are directional quantities.

This paper describes a procedure for the identification of invariant parameters governing the bending of anisotropic plates. It is shown that the whole displacement field processing of the surface strain fields obtained in two particular loading cases directly provides those parameters. A numerical simulation shows the stability of the present method. Copyright © 1996 Elsevier Science Ltd

INTRODUCTION

The determination of the whole set of rigidities of anisotropic media from only one specimen subjected to a reduced number of testing configurations is the objective of many papers. Different materials are tested: wood (Rouger *et al.*, 1990), fabric (Hendriks, 1991), corrugated paper (Mauvoisin *et al.*, 1994) and especially composite materials (for instance Mota Soares *et al.*, 1993; Grédiac and Vautrin, 1993). The papers to be found present two main types of methods based on either static or dynamic tests performed on plate specimens.

Suitable treatments of inhomogeneous strain fields provided by static tests are available for the determination of the stiffness parameters (Rouger *et al.*, 1990; Hendriks, 1991; Bezine and Shi, 1992; Grédiac and Vautrin, 1993). The whole displacement field on the surface of the plate is required for such methods. On the other hand, dynamic tests are based on the measurement of a limited number of eigenfrequencies. An objective function expressing the difference between the measured eigenfrequencies of the specimen and the corresponding eigenfrequencies provided by a numerical model is established. Various methods which minimize this function with respect to the constants to be determined have been published (Pedersen, 1989; De Wilde, 1991; Frederiksen, 1993; Mota Soares *et al.*, 1993). It must be pointed out that the unknown constants are determined indirectly with such dynamic methods.

The main advantage of the above approaches is to reduce the scatter usually induced by the use of many coupons. Moreover, the tested specimen is often a large part of a structure like a plate and local discrepancies of the mechanical properties are consequently averaged out. This opens the way to a much more effective identification of properties than is possible with the usual tests carried out on smaller coupons. For the sake of simplicity in the experimental procedure, these parameters are often measured using bending tests. Two theoretical difficulties appear, however, for solving this inverse problem. First, the strain field on the surface of the tested specimen is usually heterogeneous and no exact solutions are available to relate the unknown parameters to the measured loading, strain

or displacements components. Hence, an efficient numerical procedure is generally required to deduce the unknown parameters from the measurements. Second, considering heterogeneous strain fields allows an extra freedom for the design of the specimen shape as well as for the location of the supports and of the loading. Such a possibility can be applied to define experimental set-ups which provide the best possible identification of the parameters. This challenge is, however, difficult to face because of the anisotropy of the tested materials. For instance, a testing configuration well suited to a particular material can become less adequate if the specimen is rotated in the testing device or if another material with a different degree of anisotropy is tested. A solution is to define loading cases which would allow the determination of invariant parameters from which the directional stiffnesses or compliances are deduced (Tsai and Hahn, 1980). Such an approach partially solves the problem of the best identification of the parameters, as the invariant parameters are determined independently on the position of the plate in the testing device. Moreover, these invariant parameters describe the intrinsic elastic behavior of anisotropic materials and allow comparisons between them independently of the frame of reference.

This paper is divided into three parts. The local states of stress allowing the determination of invariant parameters are firstly presented in the case of a plane state of stress. The loading cases leading to the corresponding average states of stress will then be determined within the framework of the bending of plates. Results of various numerical simulations showing the relevancy and the stability of the present approach will also be given.

STATES OF STRESS ALLOWING THE DETERMINATION OF INVARIANT PARAMETERS

Introduction

Within the framework of plane elasticity, the strain-stress relations for an anisotropic material is written as follows:

$$\begin{pmatrix} \varepsilon_1 \\ \varepsilon_2 \\ \varepsilon_6 \end{pmatrix} = \begin{pmatrix} S_{11} & S_{12} & S_{16} \\ S_{12} & S_{22} & S_{26} \\ S_{16} & S_{26} & S_{66} \end{pmatrix} \begin{pmatrix} \sigma_1 \\ \sigma_2 \\ \sigma_6 \end{pmatrix} \tag{1}$$

The notation introduced by Tsai and Hahn (1980) can be used advantageously

$$\begin{cases} p_\varepsilon = \dfrac{\varepsilon_1 + \varepsilon_2}{2} \\ q_\varepsilon = \dfrac{\varepsilon_1 - \varepsilon_2}{2} \\ r_\varepsilon = \dfrac{\varepsilon_6}{2} \end{cases} \tag{2}$$

and

$$\begin{cases} p_\sigma = \dfrac{\sigma_1 + \sigma_2}{2} \\ q_\sigma = \dfrac{\sigma_1 - \sigma_2}{2} \\ r_\sigma = \sigma_6 \end{cases} \tag{3}$$

p_ε and p_σ are respectively the first-order invariants for strain and stress transformations. They are the coordinates of the centers of the Mohr's circles for strain and stress transformations. In the same way, the second-order invariants are the radii of these circles. They are defined as

$$\begin{cases} R_\varepsilon = \sqrt{q_\varepsilon^2 + r_\varepsilon^2} \\ R_\sigma = \sqrt{q_\sigma^2 + r_\sigma^2} \end{cases} \tag{4}$$

If we use the combinations as defined by eqns (2) and (3), eqn (1) becomes

$$\begin{pmatrix} p_\varepsilon \\ q_\varepsilon \\ r_\varepsilon \end{pmatrix} = \frac{1}{2} \begin{pmatrix} S_{11}+S_{22}+2S_{12} & S_{11}-S_{22} & S_{16}+S_{26} \\ S_{11}-S_{22} & S_{11}+S_{22}+2S_{12} & S_{16}-S_{26} \\ S_{16}+S_{26} & S_{16}-S_{26} & S_{66} \end{pmatrix} \begin{pmatrix} p_\sigma \\ q_\sigma \\ r_\sigma \end{pmatrix} \tag{5}$$

The compliances are deduced from invariant parameters described for instance by Tsai and Hahn (1980) or Verchery (1990). Such parameters reveal the effective intrinsic elastic properties of the material to be characterized. For the sake of simplicity, using the notation introduced by Verchery (1990):

$$\begin{cases} S_{11} = T_0 + 2T_1 + R_0 \cos 4a_0 + 4R_1 \cos 2a_1 \\ S_{22} = T_0 + 2T_1 + R_0 \cos 4a_0 - 4R_1 \cos 2a_1 \\ S_{12} = -T_0 + 2T_1 - R_0 \cos 4a_0 \\ S_{66} = 4(T_0 - R_0 \cos 4a_0) \\ S_{16} = 2(R_0 \sin 4a_0 + 2R_1 \sin 2a_1) \\ S_{26} = 2(-R_0 \sin 4a_0 + 2R_1 \sin 2a_1) \end{cases} \tag{6}$$

Conversely,

$$\begin{cases} T_0 = \frac{1}{8}(S_{11}+S_{22}-2S_{12}+S_{66}) \\ T_1 = \frac{1}{8}(S_{11}+S_{22}+2S_{12}) \\ R_0 e^{\pm i a_0} = \frac{1}{8}(S_{11}+S_{22}-2S_{12}-S_{66}+2i(S_{16}-S_{26})) \\ R_1 e^{2i a_1} = \frac{1}{8}(S_{11}-S_{22}+i(S_{16}+S_{26})) \end{cases} \tag{7}$$

T_0, T_1, R_0, R_1 are four invariant and independent parameters. Geometric interpretation of the above equations can be shown through two generalized Mohr's circles with radii R_0 and R_1 and rotations four and two times that of the coordinate axes (Tsai and Hahn, 1980; Verchery, 1990) (see Fig. 1). The distance between the two circles is T_0+2T_1. The locations of the centers are defined arbitrarily by T_1 and T_0+3T_1. a_0 and a_1 are changed into $a_0+\theta$ and $a_1+\theta$ under a clockwise rotation θ of the frame. The difference a_0-a_1 is therefore the fifth and last invariant. Using these linear combinations, the strain-stress relation (5) becomes

$$\begin{pmatrix} p_\varepsilon \\ q_\varepsilon \\ r_\varepsilon \end{pmatrix} = 2 \begin{pmatrix} 2T_1 & 2R_1 \cos 2a_1 & 2R_1 \sin 2a_1 \\ 2R_1 \cos 2a_1 & T_0 + R_0 \cos 4a_0 & R_0 \sin 4a_0 \\ 2R_1 \sin 2a_1 & R_0 \sin 4a_0 & T_0 - R_0 \cos 4a_0 \end{pmatrix} \begin{pmatrix} p_\sigma \\ q_\sigma \\ r_\sigma \end{pmatrix} \tag{8}$$

When a mechanical test is performed, the material is subjected to a given state of stress defined by p_σ, q_σ, r_σ. The corresponding state of strain is measured and three linear equations can be written from eqn (8). In the general case, when p_σ, q_σ and r_σ are not zero, it can be seen in eqn (8) that one cannot directly determine any set of three parameters out of the six. However, two particular states of stress will provide directly these parameters.

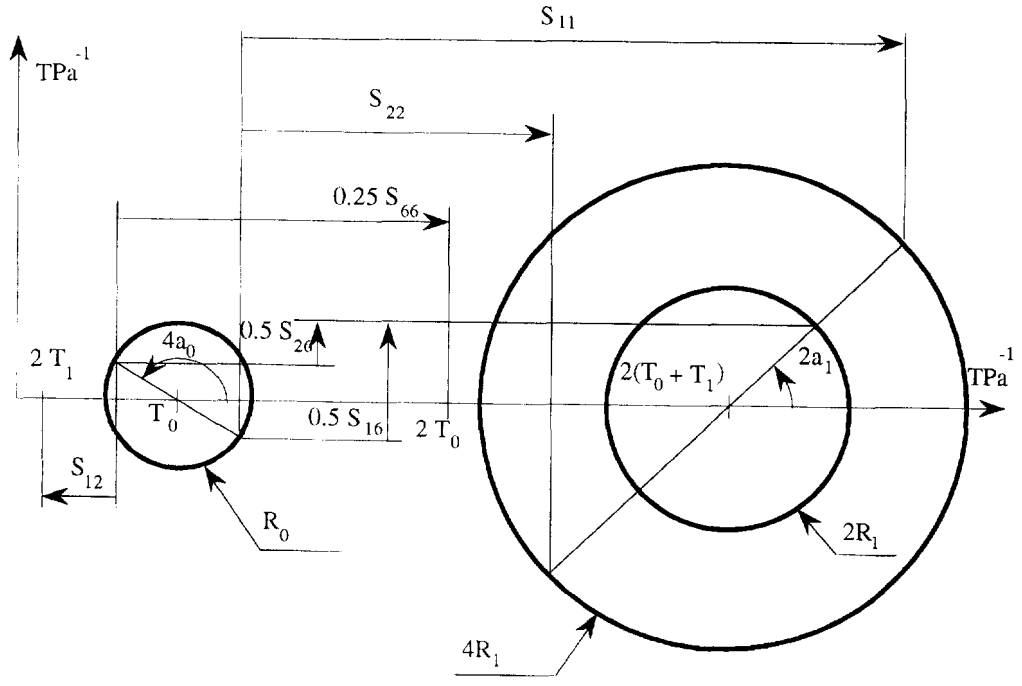

Fig. 1. Generalized Mohr's circles for compliance.

Isotropic stresses

In this case, the state of stress is such that

$$q_\sigma = r_\sigma = 0 \quad \text{and} \quad p_\sigma \neq 0 \tag{9}$$

Equation (8) becomes

$$\begin{pmatrix} p_\varepsilon \\ q_\varepsilon \\ r_\varepsilon \end{pmatrix} = 4p_\sigma \begin{pmatrix} T_1 \\ R_1 \cos 2a_1 \\ R_1 \sin 2a_1 \end{pmatrix} \tag{10}$$

Hence

$$\begin{cases} T_1 = \dfrac{p_\varepsilon}{4p_\sigma} \\ R_1 = \dfrac{R_\varepsilon}{4\text{abs}(p_\sigma)} \\ \sin(2a_1) = \dfrac{r_\varepsilon}{4R_1 p_\sigma}, \cos(2a_1) = \dfrac{q_\varepsilon}{4R_1 p_\sigma} \end{cases} \tag{11}$$

As a result, three of the six unknown, T_1, R_1 and a_1 are obtained if the material is subjected to isotropic stresses. In this case, the Mohr's circle of the strain and one of the generalized Mohr's circle are homothetic (Fig. 2).

Shear stresses

On close inspection, it can be seen in eqn (8) that the three remaining parameters T_0, R_0 and a_0 are involved only in the two last equations. Hence they cannot be directly characterized from any particular state of stress. Notice, however, that pure shear stresses lead to

$$p_\sigma = r_\sigma = 0 \quad \text{and} \quad q_\sigma \neq 0 \tag{12}$$

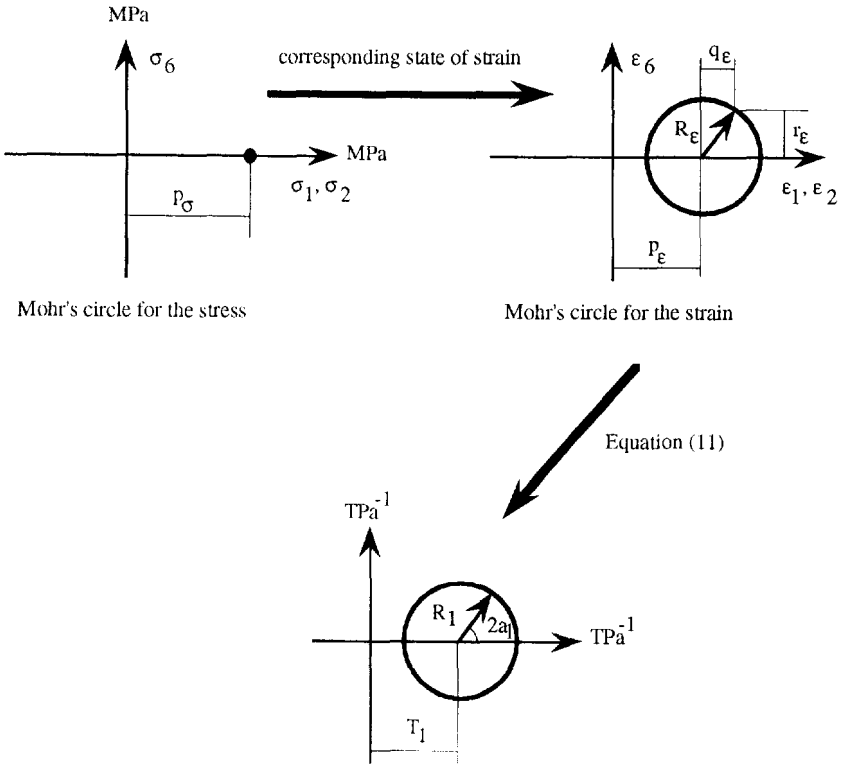

Fig. 2. First generalized Mohr's circle obtained with isotropic stresses.

In this case, eqn (8) becomes

$$\begin{pmatrix} q_\varepsilon \\ r_\varepsilon \end{pmatrix} = 2q_\sigma \begin{pmatrix} T_0 + R_0 \cos 4a_0 \\ R_0 \sin 4a_0 \end{pmatrix} \tag{13}$$

Assuming now that the same state of stress is applied to the same plate rotated through 45°, a_0 increases through 45°. Let the new state of strain be defined by p'_ε, q'_ε and r'_ε

$$\begin{pmatrix} q'_\varepsilon \\ r'_\varepsilon \end{pmatrix} = 2q_\sigma \begin{pmatrix} T_0 - R_0 \cos 4a_0 \\ -R_0 \sin 4a_0 \end{pmatrix} \tag{14}$$

The three last unknown parameters are then deduced from eqns (13) and (14) (see Fig. 3)

$$\begin{cases} T_0 = \dfrac{1}{4q_\sigma}(q_\varepsilon + q'_\varepsilon) \\ R_0 = \dfrac{1}{4\text{abs}(q_\sigma)}\sqrt{(q_\varepsilon - q'_\varepsilon)^2 + (r_\varepsilon - r'_\varepsilon)^2} \\ \sin(4a_0) = \dfrac{1}{4R_0 q_\sigma}(r_\varepsilon - r'_\varepsilon), \cos(4a_0) = \dfrac{1}{4R_0 q_\sigma}(q_\varepsilon - q'_\varepsilon) \end{cases} \tag{15}$$

In conclusion, a state of pure shear stress applied in two frames rotated through 45° is required to determine T_0, R_0 and a_0.

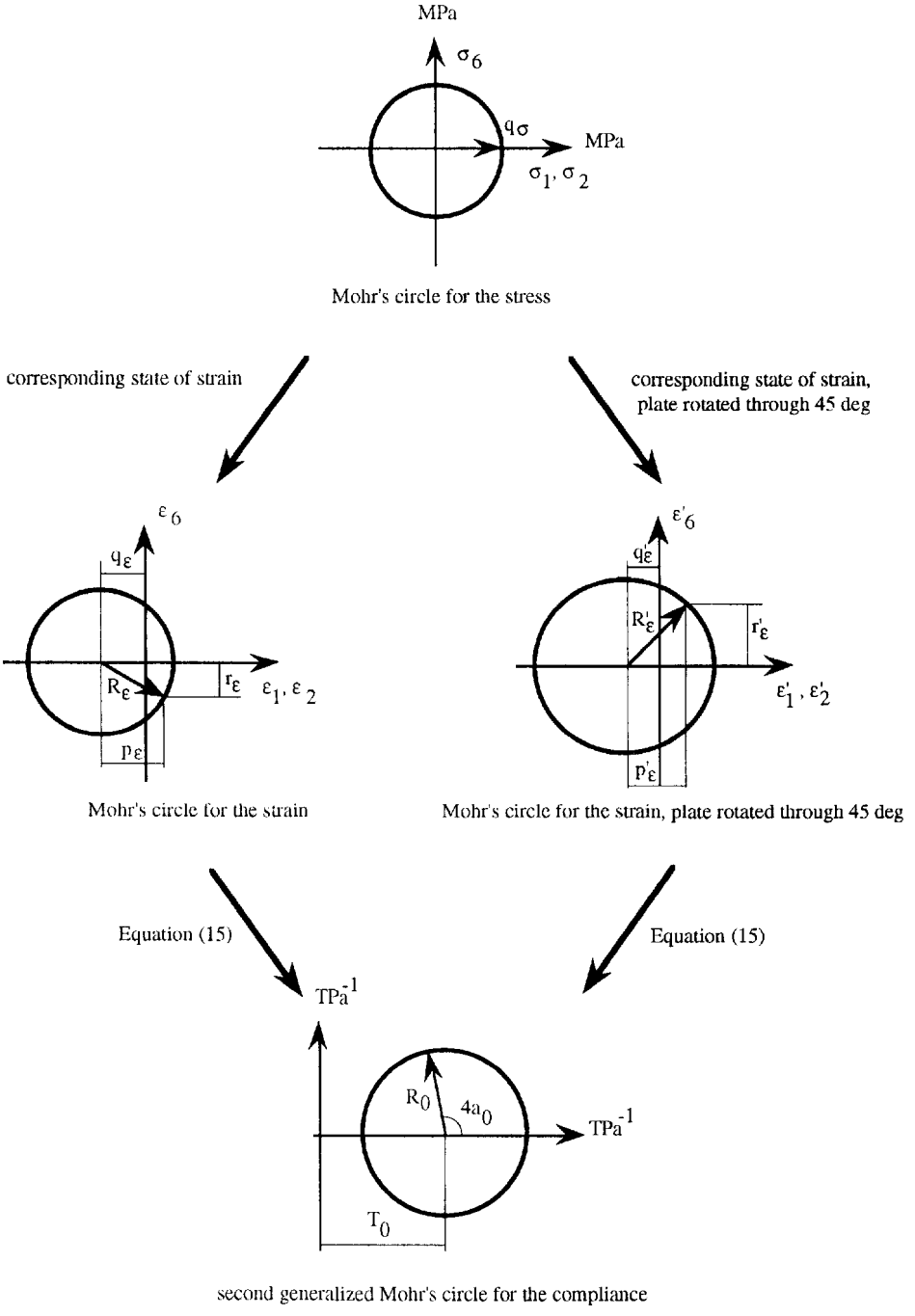

Fig. 3. Second generalized Mohr's circle obtained with two shear stress states.

PRACTICAL REALIZATION. INTRODUCTION OF AVERAGE STRESS AND STRAIN COMPONENTS

Introduction

The practical realization of the two above homogeneous states of stress on the same specimen would obviously be problematic. The idea developed here is to apply two loading cases inducing the corresponding average states of stress. The stress field is therefore heterogeneous and eqns (9) and (12) are not necessarily verified at any point.

Let $\bar{X}$ be the value of a quantity X obtained with average strain or stress components on the surface of the tested specimen

$$\bar{X} = \frac{1}{S}\int_S X \, ds \tag{16}$$

From eqns (9) and (12), one can define average isotropic stresses by

$$\overline{q_\sigma} = \overline{r_\sigma} = 0 \quad \text{and} \quad \overline{p_\sigma} \neq 0 \tag{17}$$

and average pure shear stresses by

$$\overline{p_\sigma} = \overline{r_\sigma} = 0 \quad \text{and} \quad \overline{q_\sigma} \neq 0 \tag{18}$$

Assuming the material properties are homogeneous on the whole specimen, a relationship between average strain and stress components is deduced from eqn (8)

$$\begin{pmatrix} \overline{p_\varepsilon} \\ \overline{q_\varepsilon} \\ \overline{r_\varepsilon} \end{pmatrix} = 2\begin{pmatrix} 2T_1 & 2R_1\cos 2a_1 & 2R_1\sin 2a_1 \\ 2R_1\cos 2a_1 & T_0 + R_0\cos 4a_0 & R_0\sin 4a_0 \\ 2R_1\sin 2a_1 & R_0\sin 4a_0 & T_0 - R_0\cos 4a_0 \end{pmatrix}\begin{pmatrix} \overline{p_\sigma} \\ \overline{q_\sigma} \\ \overline{r_\sigma} \end{pmatrix} \tag{19}$$

Using the two particular states of stress defined by eqns (17) and (18), eqns (11) and (15) become

$$\begin{cases} T_1 = \dfrac{\overline{p_\varepsilon}}{4\overline{p_\sigma}} \\ R_1 = \dfrac{\overline{R_\varepsilon}}{4\mathrm{abs}(\overline{p_\sigma})} \\ \sin(2a_1) = \dfrac{\overline{r_\varepsilon}}{4R_1\overline{p_\sigma}}, \cos(2a_1) = \dfrac{\overline{q_\varepsilon}}{4R_1\overline{p_\sigma}} \end{cases} \tag{20}$$

and

$$\begin{cases} T_0 = \dfrac{1}{4\overline{q_\sigma}}(\overline{q_\varepsilon} + \overline{q'_\varepsilon}) \\ R_0 = \dfrac{1}{4\overline{q_\sigma}}\sqrt{(\overline{q_\varepsilon} - \overline{q'_\varepsilon})^2 + (\overline{r_\varepsilon} - \overline{r'_\varepsilon})^2} \\ \sin(4a_0) = \dfrac{1}{4R_0 q_\sigma}(\overline{r_\varepsilon} - \overline{r'_\varepsilon}), \cos(4a_0) = \dfrac{1}{4R_0 q_\sigma}(\overline{q_\varepsilon} - \overline{q'_\varepsilon}) \end{cases} \tag{21}$$

The main feature of this approach is the requirement of the whole displacement or strain field on the surface of the specimen. From an experimental point of view, such a measurement is performed with a suitable optical method already used for such identification problems (Hendriks, 1991; Grédiac and Vautrin, 1993; Mauvoisin *et al.*, 1994). Let us now examine the loading cases which lead to the two above particular average states of stress.

Relationship between the applied forces and the average stress components on the surface of the tested plate

For the sake of simplicity in the experimental procedure, consider a plate simply supported and subjected to a normal force in M_4 as plotted in Fig. 4. Examine the relationship between the applied force and the average stress components on the surface of the plate. Note the compliances involved here are the bending compliances d_{ij}^* (Tsai and Hahn, 1980).

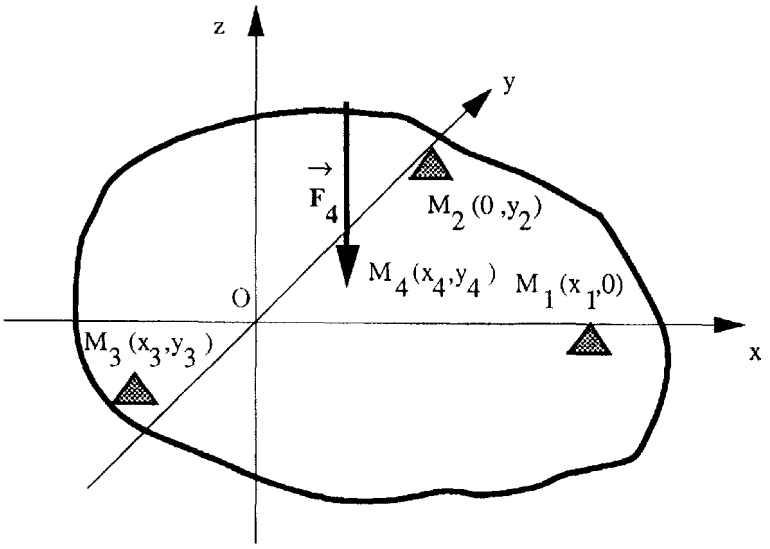

Fig. 4. Plate with normal load.

The link between the average strain and the average stress on the surface on the plate is firstly obtained integrating the strain-stress relation (1) on the whole surface of the plate and dividing by this surface:

$$\begin{pmatrix} \overline{\varepsilon_1} \\ \overline{\varepsilon_2} \\ \overline{\varepsilon_6} \end{pmatrix} = \begin{pmatrix} d_{11}^* & d_{12}^* & d_{16}^* \\ d_{12}^* & d_{22}^* & d_{26}^* \\ d_{16}^* & d_{26}^* & d_{66}^* \end{pmatrix} \begin{pmatrix} \overline{\sigma_1} \\ \overline{\sigma_2} \\ \overline{\sigma_6} \end{pmatrix} \tag{22}$$

The stress components are here the flexural stress components (Tsai and Hahn, 1980).

$$\sigma_i = \frac{6M_i}{h^2} \quad i = 1,2,6 \tag{23}$$

where M_i, $i = 1,2,6$ are the bending moment components.

The relationship between the average stress components and the applied loading is firstly obtained with the principle of virtual work for a deformable body, which states that the external and internal virtual works are equal for any compatible deflection field $\hat{w}$ (Dym and Shames, 1973). In the present case, the principle of virtual work leads to the following equation (Lekhnitskii, 1968).

$$\sum_{i=1}^{4} F_i \hat{w}_i(x_i, y_i) = \frac{h}{3} \int_S (\hat{\varepsilon}_1, \hat{\varepsilon}_2, \hat{\varepsilon}_6) \begin{pmatrix} D_{11}^* & D_{12}^* & D_{16}^* \\ D_{12}^* & D_{22}^* & D_{26}^* \\ D_{16}^* & D_{26}^* & D_{66}^* \end{pmatrix} \begin{pmatrix} \varepsilon_1 \\ \varepsilon_2 \\ \varepsilon_6 \end{pmatrix} \mathrm{d}S \tag{24}$$

where $[D^*] = [d^*]^{-1}$ is the normalized bending stiffness matrix for uncoupled plates and F_i is the force acting at $M_i(x_i, y_i)$, $i = 1 \ldots 4$. This relationship is verified for any virtual deflection field $\hat{w}$ from which the corresponding virtual surface strain components $\hat{\varepsilon}_1$, $\hat{\varepsilon}_2$ and $\hat{\varepsilon}_6$ are deduced through the Love-Kirchhoff theory. It can be shown that the three following quadratic independent virtual fields lead to the average surface strain components (Grédiac and Vautrin, 1990):

$$\begin{cases} \hat{w}_1(x,y) = x^2 + \alpha_1 x + \alpha_2 \\ \hat{w}_2(x,y) = y^2 + \beta_1 y + \beta_2 \\ \hat{w}_3(x,y) = xy + \gamma_1 x + \gamma_2 y + \gamma_3 \end{cases} \tag{25}$$

where α_i, β_i and γ_j, $i = 1 \ldots 2$, $j = 1 \ldots 3$, are constant. It must be pointed out that the choice of these constants has no importance in the present case because they induce rigid solid virtual motions that give a zero virtual work as the plate is in equilibrium. Equation (24) written with the three above virtual fields leads to

$$\begin{pmatrix} \overline{\varepsilon_1} \\ \overline{\varepsilon_2} \\ \overline{\varepsilon_6} \end{pmatrix} = \frac{-3}{Sh^2} \begin{pmatrix} d_{11}^* & d_{12}^* & d_{16}^* \\ d_{12}^* & d_{22}^* & d_{26}^* \\ d_{16}^* & d_{26}^* & d_{66}^* \end{pmatrix} \begin{pmatrix} \sum_{i=1}^{4} F_i \hat{w}_1(x_i,y_i) \\ \sum_{i=1}^{4} F_i \hat{w}_2(x_i,y_i) \\ \sum_{i=1}^{4} F_i \hat{w}_3(x_i,y_i) \end{pmatrix} \tag{26}$$

The relationship between the forces and the surface average stress is then deduced from eqns (22) and (26):

$$\begin{pmatrix} \overline{\sigma_1} \\ \overline{\sigma_2} \\ \overline{\sigma_6} \end{pmatrix} = \frac{-3}{Sh^2} \begin{pmatrix} \sum_{i=1}^{4} F_i \hat{w}_1(x_i,y_i) \\ \sum_{i=1}^{4} F_i \hat{w}_2(x_i,y_i) \\ \sum_{i=1}^{4} F_i \hat{w}_3(x_i,y_i) \end{pmatrix} \tag{27}$$

The plate is in equilibrium, then forces F_i, $i = 1 \ldots 3$, are given as a function of the applied force F_4 and the coordinates of points M_i, $i = 1 \ldots 4$:

$$\begin{cases} F_1 = \dfrac{-F_4}{x_1}(x_4 + Kx_3) \\ F_2 = \dfrac{-F_4}{y_2}(y_4 + Ky_3) \\ F_3 = KF_4 \end{cases} \tag{28}$$

with

$$K = \frac{-x_1y_2 + x_1y_4 + x_4y_2}{x_1y_2 - x_1y_3 - x_3y_2} \tag{29}$$

The surface average stress components are then expressed as a function of the applied force F_4

$$\begin{pmatrix} \overline{\sigma_1} \\ \overline{\sigma_2} \\ \overline{\sigma_6} \end{pmatrix} = \frac{-3F_4}{Sh^2} \begin{pmatrix} Kx_3(x_3 - x_1) + x_4(x_4 - x_1) \\ Ky_3(y_3 - y_2) + y_4(y_4 - y_2) \\ Kx_3y_3 + x_4y_4 \end{pmatrix} \tag{30}$$

Forming the combinations $\overline{p_\sigma}$, $\overline{q_\sigma}$ and $\overline{r_\sigma}$ defined in eqn (3)

$$\begin{pmatrix} \overline{p_\sigma} \\ \overline{q_\sigma} \\ \overline{r_\sigma} \end{pmatrix} = \frac{-3F_4}{2Sh^2} \begin{pmatrix} C_1 \\ C_2 \\ C_3 \end{pmatrix} \tag{31}$$

with

$$\begin{pmatrix} C_1 \\ C_2 \\ C_3 \end{pmatrix} = \begin{pmatrix} K[x_3(x_3-x_1)+y_3(y_3-y_2)]+x_4(x_4-x_1)+y_4(y_4-y_2) \\ K[x_3(x_3-x_1)-y_3(y_3-y_2)]+x_4(x_4-x_1)-y_4(y_4-y_2) \\ 2(Kx_3y_3+x_4y_4) \end{pmatrix} \tag{32}$$

Parameters C_i only depend on the location of the supports and of the applied loading. Substituting eqn (31) into eqns (17) and (18) leads to the relations that must verify the coordinates of points M_i, $i = 1 \ldots 4$, to obtain the two particular average states of stress giving directly the invariant parameters.

Particular configurations leading to the invariant parameters in bending

The average isotropic surface stresses defined in eqn (17) are obtained if parameters C_i, $i = 1 \ldots 3$, verify

$$C_1 \neq 0, \quad C_2 = 0, \quad C_3 = 0 \tag{33}$$

Introducing the coordinates of points M_i, $i = 1 \ldots 4$, eqn (33) becomes

$$\begin{cases} K[x_3(x_3-x_1)+y_3(y_3-y_2)]+x_4(x_4-x_1)+y_4(y_4-y_2) \neq 0 \\ K[x_3(x_3-x_1)-y_3(y_3-y_2)]+x_4(x_4-x_1)-y_4(y_4-y_2) = 0 \\ Kx_3y_3+x_4y_4 = 0 \end{cases} \tag{34}$$

In the same way, the average shear stress state is obtained if parameters C_i, $i = 1 \ldots 3$, verify

$$C_1 = 0, \quad C_2 \neq 0, \quad C_3 = 0 \tag{35}$$

Introducing the co-ordinates of points M_i, $i = 1 \ldots 4$, eqn (35) becomes

$$\begin{cases} K[x_3(x_3-x_1)+y_3(y_3-y_2)]+x_4(x_4-x_1)+y_4(y_4-y_2) = 0 \\ K[x_3(x_3-x_1)-y_3(y_3-y_2)]+x_4(x_4-x_1)-y_4(y_4-y_2) \neq 0 \\ Kx_3y_3+x_4y_4 = 0 \end{cases} \tag{36}$$

These two sets of three equations, linking the six coordinates, characterize the two types of mechanical configurations from which the invariant parameters are determined using the procedure defined in the above sections. Only a particular case can however be reasonably studied in more detail. Assume, for instance, that the support M_3 is located on the y-axis, i.e. $x_3 = 0$. Equation (34) reduced to

$$\begin{cases} y_3y_2 = -x_1x_4 \\ y_4 = 0 \end{cases} \tag{37}$$

and eqn (36) to

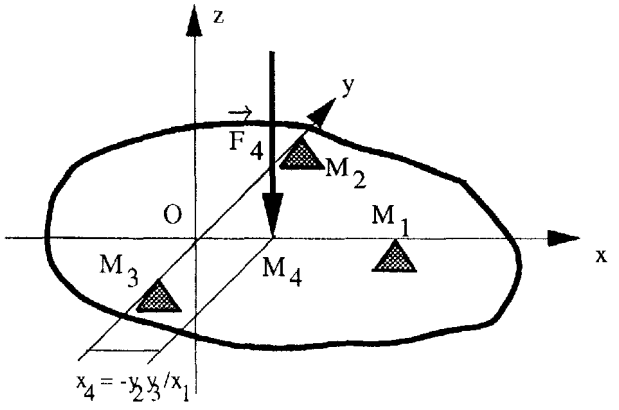

Fig. 5. Example of loading case leading to average isotropic stresses.

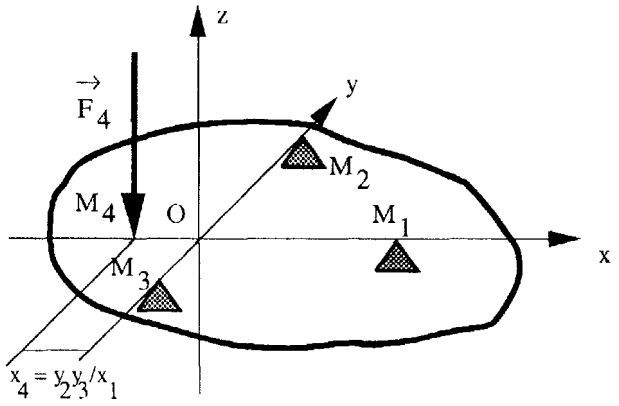

Fig. 6. Example of loading case leading to average shear stresses.

$$\begin{cases} y_3 y_2 = x_1 x_4 \\ y_4 = 0 \end{cases} \tag{38}$$

Two examples of such loading cases are plotted in Figs 5 and 6. Note that the anticlastic bending (Lekhnitskii, 1968) is a particular case of eqn (38) in which $y_3 = -y_2 = -x_1 = x_4$.

In conclusion, it has been shown that two basic mechanical configurations allow the direct determination of the unknown invariant parameters. This approach will now be tested using numerical simulations.

NUMERICAL SIMULATIONS

The aim of this section is to validate the present identification procedure and to examine the sensitivity of the identified parameters on errors in the displacement field. Notice the above procedure is valid for thin plates of any shape. However the shape of the tested specimen is here a square for the sake of simplicity in the numerical simulations. The plate is made of unidirectional graphite/epoxy, which compliances are given in Table 1.

Table 1. Normalized bending compliances used for the simulations

d_{11}^* TPa^{-1}	d_{22}^* TPa^{-1}	d_{12}^* TPa^{-1}	d_{66}^* TPa^{-1}	d_{16}^* TPa^{-1}	d_{26}^* TPa^{-1}
7.25	111.11	−2.17	140.85	0	0

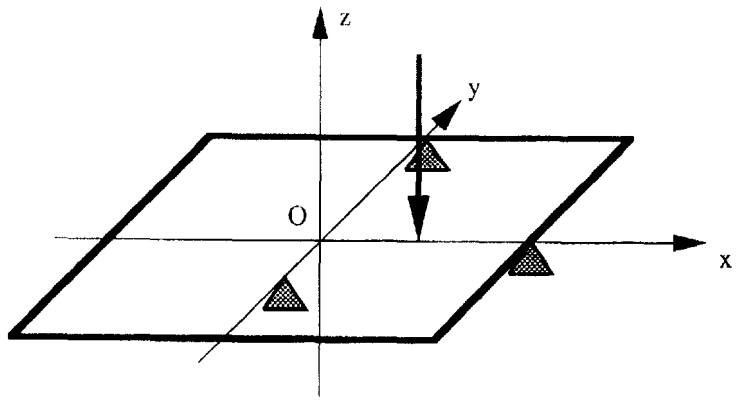

Fig. 7. Loading case 1 simulated with the finite element method.

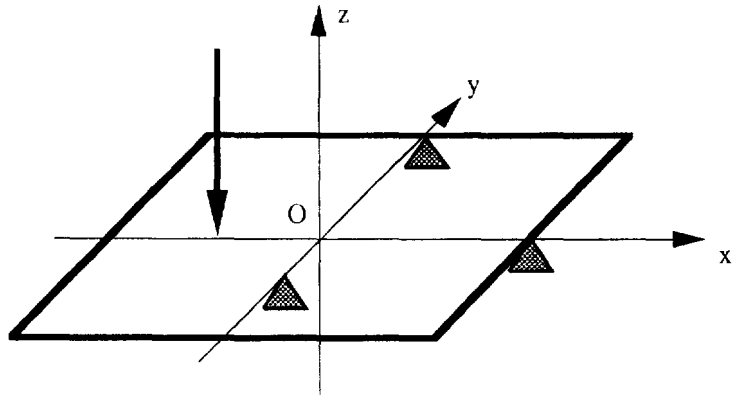

Fig. 8. Loading case 2 simulated with the finite element method.

The dimensions are $200 \times 200 \times 1$ mm^3. The two loading cases shown in Figs 7 and 8 are simulated using a finite element model. The magnitude of the force is 100 N. The location of the supports is respectively:

$$\text{loading case 1}: \quad M_1(100,0)M_2(0,100)M_3(0,-50)M_4(50,0)$$

$$\text{loading case 2}: \quad M_1(100,0)M_2(0,100)M_3(0,-50)M_4(-50,0)$$

The plate specimen is meshed with 60×60 or 62×62 rectangular elements according to the location of the plate on the supports such that the loading points and the supports match some nodes of the mesh. Each element is then divided in triangular elements based on Love-Kirchhoff plate theory (Clough and Tocher, 1965; Zienkiewicz, 1989b). Each node has therefore three degrees of freedom: the deflection w and the two slopes θ_x and θ_y.

In the first loading case defined in Fig. 7, the x-y basis matches the orthotropy basis. In the second loading case defined in Fig. 8, the x-y basis matches the orthotropy basis for the first simulation. It is then rotated through 45 deg for the second simulation.

Parameters C_i, $i = 1 \ldots 3$, are firstly computed for the two loading cases using eqn (32) (Table 2). The three linear average stress combinations $\overline{p_\sigma}$, $\overline{q_\sigma}$ and $\overline{r_\sigma}$ are then deduced using

Table 2. Parameters C_i for the two loading cases

	C_1 m^2	C_2 m^2	C_3 m^2
loading case 1	-5×10^{-3}	0	0
loading case 2	0	15×10^{-3}	0

Table 3. Average stress combinations for the two loading cases

	$\overline{p_\sigma}$ MPa	$\overline{q_\sigma}$ MPa	$\overline{r_\sigma}$ MPa
loading case 1	−18.75	0	0
loading case 2	0	56.25	0

Table 4. Average strain combinations for the two loading cases. The orthotropy basis matches the (x, y) basis (n.s. = not significant, i.e. the magnitude of the strain component is less than 1×10^{-6})

	$\overline{p_\varepsilon}$ 10^{-6}	$\overline{q_\varepsilon}$ 10^{-6}	$\overline{r_\varepsilon}$ 10^{-6}
loading case 1	−1069	974	n.s.
loading case 2	−2921	3451	n.s.
loading case 2, plate rotated through 45	n.s.	n.s.	−3990

eqn (31) (Table 3). It must be emphasized that these quantities only depend on the location of points M_i: they are not influenced by the material. The three linear strain combinations $\overline{p_\varepsilon}$, $\overline{q_\varepsilon}$ and $\overline{r_\varepsilon}$ are computed from the surface displacement field which is directly related to the two rotation fields θ_x and θ_y according to the Love-Kirchhoff theory. Hence, the element used for computing these integrals is a simple bilinear displacement rectangular element with four nodes and two degrees of freedom by node: θ_x and θ_y (Zienkiewicz, 1989a). The mesh is the same as that used for the finite element computations. The results are given in Table 4.

It is also necessary to estimate the effect of measurement errors on the parameters. Hence the rotations θ_x and θ_y provided by the finite element model at each node of the mesh are modified as follows

$$\theta_i = \theta_i(1+\delta), \quad i = x,y \tag{39}$$

where δ is a random number of magnitude A.

The parameters are computed applying the present procedure. The results are listed in Table 5. Four sets of simulations are performed: $\delta = 0$, 1%, 5% and 10%. As may be seen, five out of the six parameters are identified very precisely in the case $\delta = 0$. Only R_0 presents a difference of 6.2%. This is probably due to the small influence of this parameter on the global response of the plate when it is bent. It appears then that the sensitivity is different from one parameter to another when the magnitude of the random errors increases. Apart from R_0 already discussed, the whole set of parameters is determined with an error less

Table 5. Actual and identified parameters

	T_0 TPa^{-1}	T_1 TPa^{-1}	R_0 TPa^{-1}	R_1 TPa^{-1}	a_0 deg	a_1 deg
actual	32.94	14.25	2.26	12.98	45.00	90.00
identified, $A = 0\%$	33.07	14.25	2.40	12.98	45.00	90.00
error	0.4%	0%	6.2%	0%	0%	0%
identified, $A = 1\%$	33.17	14.34	2.45	13.02	45.01	89.97
error	0.7%	0.6%	8.4%	0.3%	0.02%	−0.03%
identified, $A = 5\%$	33.58	14.69	2.65	13.18	45.02	89.86
error	1.9%	3.1%	17.26%	1.54%	0.04%	−0.16%
identified, $A = 10\%$	34.09	15.13	2.91	13.38	45.04	89.71
error	3.49%	6.18%	28.76%	3.08%	0.08%	−0.3%

than 6.18% when $A = 10\%$. As a result, the method appears to be only slightly dependent on experimental errors.

CONCLUSION

A strategy for the direct determination of invariant parameters governing the bending of anisotropic plates has been developed and simulated using a finite element model. The main advantage of the present approach is to provide invariant parameters that describe the intrinsic nature of the mechanical behavior of the tested plate, even if it is anisotropic. From a partical point of view, it has been shown that two fundamental types of testing configurations carried out on the same specimen emphazise the contribution of those invariant parameters. The present method also provides the parameters directly. This feature avoids iterative calculations with initial guesses usually proposed in mixed numerical/experimental methods available in the literature.

This paper has included only numerically simulated experiments and is purely theoretical. The practical application requires the experimental measurement of the whole strain field on the surface of the plate specimen. Such measurements can be performed with optical methods like moiré already used in similar applications. It is worth pointing out the accuracy of the identified parameters from numerical tests and the low dependence on simulated experimental errors. This due to the fact that average strain components are considered. This last property shows that the present approach can reasonably be implemented in practice.

REFERENCES

Bezine G. and Shi G. (1992). A new method for the determination of the flexural rigidity of an orthotropic plate. *Engng Anal. Boundary Elements* **10**, 307–312.

Clough R. W. and Tocher J. L. (1965). Finite element stiffness matrices for analysis of plates in bending. In *Proc. Conf. on Matrix methods in Structural Mechanics*, AFFDL TR 66-80, Air Force Institute of Technology, Wright-Patterson AF Base, Ohio, pp. 515–546.

De Wilde W. P. (1991). Identification of the rigidities of composite systems by mixed numerical/experimental methods. In *Mechanical Identification of Composites* (eds A. Vautrin and H. Sol). Elsevier Science Publishers, pp. 1–15.

Dym C. L. and Shames D. (1973). *Solid Mechanics, a Variational Approach*. International Students Edition, Tokyo.

Frederiksen P. S. (1993). Natural vibrations of free thick plates and identification of transverse shear moduli. In *Optimal Design with Advanced Materials* (ed. P. Pedersen) Elsevier Science Publishers, pp. 131–148.

Grédiac M. and Vautrin A. (1990). A new method for determination of bending rigidities of anisotropic plates. *ASME J. Appl. Mech.* **57**, 964–968.

Grédiac M. and Vautrin A. (1993). Mechanical characterization of anisotropic plates, experiments and results. *Eur. J. Mech. A Solids* **12**, 819–838.

Hendriks M. A. N. (1991). Identification of the mechanical properties of solid materials. PhD thesis, Eindhoven University of Technology.

Lekhnitskii S. G. (1968). *Anisotropic Plates*. Gordon and Breach Science Publishers.

Mota Soares C. M., Freitas J. M., Araujo A. L. and Pedersen P. (1993). Identification of material properties of composite plate specimens. *Comp. Struc.* **25**, 277–285.

Mauvoisin G., Brémand F. and Lagarde A. (1994). Quasi-heterodyne shadow moiré. In *Proc. 10th. Conf. on Exp. Mech.*, 18–22 July 1994, Lisbon, Ed. Balkema, pp. 245–250.

Pedersen P. (1989). *Optimization Method Applied to Identification of Material Parameters, Descretization Methods and Structural Optimization Procedures and Applications* (eds H. A. Eschenauer and G. Thierauf). Springer-Verlag, Berlin, pp. 277–283.

Rouger F., Khebibeche M. and Le Govic C. (1990). Non determined tests as a way to identify wood elastic parameters: the finite element approach. In *Proc. Euromech Colloquium* 269 *Mechanical Identification of Composites*, Elsevier, pp. 82–90.

Tsai S. W. and Hahn H. T. (1980). *Introduction to Composite Materials*. Technomic.

Verchery G. (1990). Designing with anisotropy. In *Proc. Int. Conf. Textile Composites in Building Construction*, Lyon, Part 3, pp. 29–42. Plunalis, Paris.

Zienkiewicz, O. C. (1989a). *The Finite Element Method, Volume* 1, Fourth edition, McGraw-Hill, London.

Zienkiewicz, O. C. (1989b). *The Finite Element Method, Volume* 2, Fourth edition, McGraw-Hill, London.